

# Long-term incubations reveal geochemical controls on wood biomass preservation at the anoxic sediment-water interface

Amiel N.,1# Rubin-Blum M.,2,3 Lahovitski H.,1,3 Krost P.,1,4 and Angel D.L.,1,3

This is a non-peer-reviewed preprint submitted to EarthArXiv.

<sup>&</sup>lt;sup>1</sup> Rewind Earth LTD

<sup>&</sup>lt;sup>2</sup> Biology Department, Israel Oceanographic and Limnological Research Institute, Haifa, Israel

<sup>&</sup>lt;sup>3</sup> Department of Maritime Civilizations & Recanati Institute for Maritime Studies, University of Haifa, Haifa, Israel

<sup>&</sup>lt;sup>4</sup> CRM - Coastal Research & Management LTD, Kiel, Germany

<sup>#</sup> Corresponding author. E-mail: nitai@rewind.earth



#### **Abstract**

Ocean-based carbon dioxide removal (CDR) strategies increasingly consider biomass burial in anoxic marine basins as a pathway for long-term carbon storage. To evaluate its stability and environmental impact, we conducted 14-month bottle incubations testing three configurations of terrestrial wood under anoxic conditions: suspended in the water column, placed on the sediment surface, and buried within sediments. Across all treatments, wood remained highly preserved: >97.5% carbon retained, based on C content, ~98.3% via carbon budgets, and >96% based on dry mass retained. Geochemical signals indicated that sulfate reduction was the dominant terminal pathway: dissolved inorganic carbon and alkalinity increased in nearly a 1:1 stoichiometry, methane yields were low relative to Dissolved Inorganic Carbon (DIC), and sulfide was presumably sequestered into iron sulfide minerals. Microbial community analyses corroborated these patterns, showing enrichment of fermenters and sulfate reducers with only minor contributions from methanogens. Dissolved organic carbon (DOC) dynamics further revealed sediment contact as a key control on DOC retention, with suspended wood yielding the most significant DOC accumulation. We observed no mobilization of toxic metals and only minor changes in major cations during the 14 months. Together, these results demonstrate that geochemical and microbial processes act in concert to preserve biomass carbon under anoxic conditions, highlighting marine burial as a durable, low-risk CDR strategy.

#### 1. Introduction

Climate change poses a significant threat to ecosystems worldwide, driven by the accumulation of carbon dioxide (CO<sub>2</sub>) in the atmosphere. Combating it requires substantial carbon dioxide removal (CDR) in parallel with decarbonization and emission reductions (IPCC, 2023). Marine CDR is an emerging solution that leverages the oceans' natural ability to sequester carbon (National Academies of Sciences, Engineering, and Medicine, 2021). One such method involves depositing terrestrial biomass into oxygen-free (anoxic) marine environments, where reduced decomposition rates enable carbon to remain stored for centuries and even millennia (Keil et al., 2010; Raven et al., 2023, and references therein).

In anoxic environments, microbes drive the decomposition of organic matter through processes such as sulfate reduction, methanogenesis, and iron reduction (Canfield, 1994; Beulig et al., 2017;



Reeburgh, 2007). A simplified conceptual model of organic matter degradation in anoxic marine sediments involves the stepwise mineralization of reactive components in the particulate organic carbon (POC) pool (Fenchel and Finlay 1995; Canfield et al., 2005). This process begins with hydrolysis, which converts POC into dissolved organic carbon (DOC), forming substrates available for further microbial processing (Hee et al., 2001). In sulfate-reducing and methanogenic environments, hydrolysis products are fermented by intermediate microbial consortia rather than directly by sulfate reducers or methanogens, leading to the production of volatile organic acids such as acetate and formate (Canfield et al., 2005). These fermentation products are subsequently oxidized by sulfate-reducing and methanogenic microorganisms, resulting in the production of dissolved inorganic carbon (DIC) and methane (CH<sub>4</sub>) through terminal metabolism (Beulig et al., 2017; Reeburgh, 2007). This sequence of coupled metabolic processes determines both the rate and efficiency of organic carbon mineralization and the preservation of organic matter in marine sediments (Canfield, 1994). The breakdown of organic carbon releases various molecules into the surrounding water, including DOC, DIC, as well as other metabolic byproducts like hydrogen sulfide (H<sub>2</sub>S), methane, and ferrous iron (Jørgensen, 2000). These changes in the water's chemical composition reflect the complex interactions between organic matter and microbial communities that mediate its decomposition in the absence of oxygen.

The chemistry of the biomass and the composition of ambient microbial communities influence its decomposition in anoxic sediments. Decomposition pathways differ between anoxic waters and anoxic sediments because of contrasting environmental conditions and microbial activities (Middelburg & Levin, 2009; Treude, 2011). The water column provides a dynamic environment in which organic compounds can disperse. In contrast, anoxic sediments offer a more stable environment, where organic matter remains buried and in close contact with sediment particles, resulting in distinct microbial and geochemical interactions (Gobas & MacLean, 2003). While major ions, such as sulfate, are present at high concentrations in seawater, their availability to microbes differs significantly between the water column and sediments. In sediments, sulfate is confined to narrow pore spaces where slow diffusion severely limits its replenishment. This transport process is far more restricted than in the overlying water column, even in stratified, non-mixing zones, resulting in significantly lower sulfate availability and promoting distinct microbial metabolisms.



To investigate the potential of marine biomass storage as a carbon sequestration strategy, we conducted an experiment testing the decomposition of lignocellulosic terrestrial biomass (wood) under three distinct anoxic conditions: (1) suspension in the water column, (2) deposition on the seafloor, and (3) burial within the sediment. We hypothesized that decomposition rates and microbial transformations of terrestrial biomass differ significantly depending on the anoxic microenvironment. Specifically, we ask: How do the rates and extents of lignocellulosic biomass degradation vary across these three anoxic conditions? How do microbial community composition and functional activity respond to the introduction of wood in each setting? To what extent does each experimental setting promote carbon retention versus loss?

#### 2. Materials and Methods

# 2.1 Experimental setup

We conducted the experiment using 114 mL crimp-seal anoxic bottles, incubated for 410 days. Each bottle was filled with 30 mL of sediment and 60 mL of anaerobic seawater, with salinity adjusted to 20 ppt by diluting Mediterranean seawater with double-distilled water (DDW). A 10-minute flushing with N<sub>2</sub> gas followed this to establish anaerobic conditions. Butyl Rubber stoppers (20 mm), to which beech wood pieces were attached, were then inserted into the bottles, positioning the wood according to the desired configuration: wood in the water column, wood placed on the sediment-water interface, or wood buried within the sediment. The wood pieces were affixed to plastic sticks of varying lengths, depending on the specific configuration, and these sticks were subsequently attached to the rubber stoppers used to seal the bottles (Figure 1). Woodfree control bottles contained only the plastic sticks without any wood attached. The bottles were subsequently sealed with an aluminum cap using a crimper. At each sampling interval, 12 bottles were examined, with three replicates for each configuration (wood in the water column, wood on the sediment-water interface, wood buried within the sediment), as well as wood-free controls.





Figure 1. A) Wood piece attached to a plastic stick. B) Wood placement in different configurations.

#### 2.2 Sediment and seawater collection and handling

Sediments were collected from the silty/muddy Mediterranean seafloor at a depth of 80 m using a box corer during a cruise aboard the R/V Yanikam on December 3, 2023. We removed the upper 4 cm of sediment in the box core, and the remaining sediment was homogenized and stored in sealed containers until processed. Seawater was collected from the Mediterranean Sea shore, next to Nitzanim beach (31°44'45"N/34°36'02"E), on February 3, 2024. The water was filtered through a 1 mm mesh, diluted (salinity-adjusted) using distilled water to a salinity of 20 ppt, similar to the salinity in the deep Black Sea, and then flushed with N<sub>2</sub> gas until oxygen was depleted (anoxic seawater). Oxygen concentrations were measured using a Hach oxygen optode (Intellical LDO101, connected to a Hach HQ 4000).

#### 2.3 Biomass collection and configuration

To assess the extent of wood preservation under experimental conditions, we applied four independent methods: i) visual assessment of wood breakdown, ii) measurement of dry mass loss, iii) measurement of wood carbon content, and iv) measurements of C budget of the decomposition products. We sectioned Beech wood into  $0.8 \times 0.8 \times 1$  cm blocks, sized to fit the narrow necks of the glass bottles used in the experiment. Each piece of wood was weighed with 0.1 mg precision. Initial water content in five representative wood samples was determined for dry mass loss calculations (method ii), and changes in carbon content (method iii).



To quantify loss of wood carbon (method iii), we calculated the carbon budget by summing all carbon released as dissolved inorganic carbon ( $C_{DIC}$ ), dissolved organic carbon ( $C_{DOC}$ ), and methane ( $C_{CH_4}$ ) in our anoxic incubation bottles. For each 400 mg piece of wood (184 mg C, 46% C by mass), we calculated the change in concentration ( $\Delta C$ ) from Day 0 to Day 410. Concentration changes (mM for DIC/DOC;  $\mu$ M for CH<sub>4</sub>) were converted to mmol C ( $\Delta C \times 0.06$  L) and then to mg C ( $\times 12$  mg C mmol L<sup>-1</sup>). We estimated the percentage of wood carbon loss as a sum of  $C_{DIC}$ ,  $C_{DOC}$ , and  $C_{CH_4}$ , divided by the initial 184 mg.

#### 2.4 Sampling and measurements

We sampled the headspace in the experimental bottles using a gas-tight Pressure Lok Glass Syringe and transferred it to 10 mL gas-tight vials. Methane concentrations in the vials were analyzed using gas chromatography coupled with flame ionization detection (GC-FID; Thermo). We collected water samples from the anoxic bottles at the start of the experiment, before biomass addition, and at each sampling interval (6, 19, 61, 131, 202, 322, and 410 days) for sulfide concentration, alkalinity (acid-base titration, Titroline 7000), dissolved inorganic carbon (DIC analyzer model AS-C6L, Apollo, which included a laser-based CO2 detector model LI-7815, LI-COR), and dissolved organic carbon (TOC-VCPH Total Organic Carbon analyzer; Shimadzu, Kyoto, Japan). We analyzed major ions on days 61 and 420, using ion chromatography (881 Compact IC pro; Metrohm AG, Switzerland). Water samples for all analyses, except dissolved organic carbon (DOC), were prefiltered using 0.45 µm PVDF filters, while DOC samples were filtered with 0.7 µm GFF filters. Samples for sulfide analysis were preserved with a 2.6% (v/v) zinc acetate solution, frozen at -20°C, and collectively thawed and measured using spectrophotometry (Cline, 1969) after the 131- and 410-day sampling intervals. Following the removal of overlying water, 1-gram samples were collected from the sediment surface ("top") and from the homogenized bulk sediment ("mix"), and stored in sterile 1.5 mL cryovials at -80 °C pending DNA extraction.

## 2.5 DNA extraction and sequencing

DNA was extracted from samples using 270 µl GT lysis buffer and 30 µl proteinase K (from MagCore Genomic DNA Tissue Kit) along with 200 µl sample in type C bead-beating tubes (GeneAid). Bead beating was performed for 2 minutes using a Biospec machine. Samples were



then incubated at 60°C for 2 hours and extracted using the MagCore machine (RBC Bioscience) with MagCore Genomic DNA Tissue Kit cartridges and protocol.

Sequencing targeted the 16S rRNA gene using standard high-throughput protocols. Two microliters of DNA were used as the template for the initial polymer chain reaction (PCR). Amplification was conducted on the V4 region (~300 bp) of the 16S rRNA gene using PCRbio Hot Start Ready Mix with the 515F/806R primers (Apprill et al., 2015; Parada et al., 2016), amended with CS1/CS2 adaptors, for 25 cycles. 2 μl of the PCR product was amplified for 10 cycles in 10 μl using the Fluidigm Access Array Barcode library, according to the manufacturer's protocol (2 μl of barcode per reaction). DNA was purified using Kapa Pure Beads at a 0.65X ratio and quantified with Qubit using the Denovix DsDNA High Sensitivity Assay. Samples were sequenced with MiSeq (Illumina), with 30% PhiX using MiSeq Reagent Kit v2 500PE. We demultiplexed the reads using bcl2fastq with default parameters, allowing for zero mismatches. The data was then mapped to PhiX using Bowtie2 to remove PhiX control and unmapped reads, which were quantified, collected, and examined using FastQC.

Demultiplexed reads were analyzed using the CLC Genomics Workbench (Qiagen) and the microbiome pipeline with default settings. The adaptors were removed and the reads with a quality score lower than 25 or length <150 were discarded. The maximum number of acceptable ambiguous nucleotides was set to 2 and the length of the reads was fixed at 200–500bp. Chimeric sequences and singletons were detected and discarded. We clustered the reads into OTUs following the alignment to the SILVA database at 97% sequence similarity. The OTUs were classified using a Scikit-Learn classifier trained on the Silva database v138.1 (Glöckner et al., 2017). Downstream analyses were performed in R v4.1.1 (R Core Team, 2024), using packages Phyloseq (McMurdie and Holmes, 2013) and Ampvis2 (Andersen et al., 2018). After removing mitochondrial and chloroplast sequences, we explored the community composition through alpha diversity indices, Principal Coordinates Analysis (PCoA) on Bray-Curtis dissimilarities, and pairwise PERMANOVA. We tested for significant shifts in community structure and identified indicator taxa using indispecies package v1.7.9 (De Cáceres et al., 2012), as well DESeq2 (Love et al., 2014). To investigate functional shifts in the microbial communities, we used PICRUSt2 (Douglas et al., 2020; Wright and Langille, 2025) to infer potential metabolic pathways based on the 16S rRNA gene profiles. Both KEGG Orthologs (KOs) and MetaCyc pathways were analyzed



using DESeq2 to identify features significantly different between control and wood-amended treatments. Amplicon reads were deposited in the NCBI SRA archive under project number PRJNA1338952 (https://doi.org/10.5281/zenodo.17640300).

#### 3. Results and Discussion

#### 3.1 Wood additions resulted in methane release

Our results indicate a significant disparity between the bottles containing wood and the controls (no wood addition), with very low methane production observed in the latter (Figure 2A). At the final incubation stage (day 410), methane concentrations in all wood treatments were markedly higher than in the control, as confirmed by statistical analysis ( $t_{(2)} = 6.4-15.9$ , p < 0.05). Among the wood-containing configurations, the sediment-buried wood exhibited the highest methane production within the first 61 days. Between 61 and 410 days, methane levels increased across all configurations, with the buried wood and wood on the sediment surface showing slightly higher concentrations, while bottles with wood in the water column had lower methane concentrations. The results suggest that the extent of contact between the biomass and sediment, where diverse microbial communities reside (e.g., Lovley & Phillips, 1987; Megonigal et al., 2003), and where redox potential and diffusive fluxes of sulfate are decreasing (Froelich et al., 1979; Berner, 1981), may enhance methane production. Similar relationships between sediment-organic matter coupling, sulfate depletion, and stimulation of methanogenesis have been reported in marine and lacustrine anoxic systems (Crill & Martens, 1986; Maltby et al., 2018). Our results suggest noncompetitive, methylotrophic methanogenesis, as sulfate concentrations in the overlying water of the experimental systems remained high (see Section 3.5). It is plausible that the observed methane production occurred in parallel with sulfate reduction (Oremland and Polcin, 1982; Sela-Adler et al., 2015).



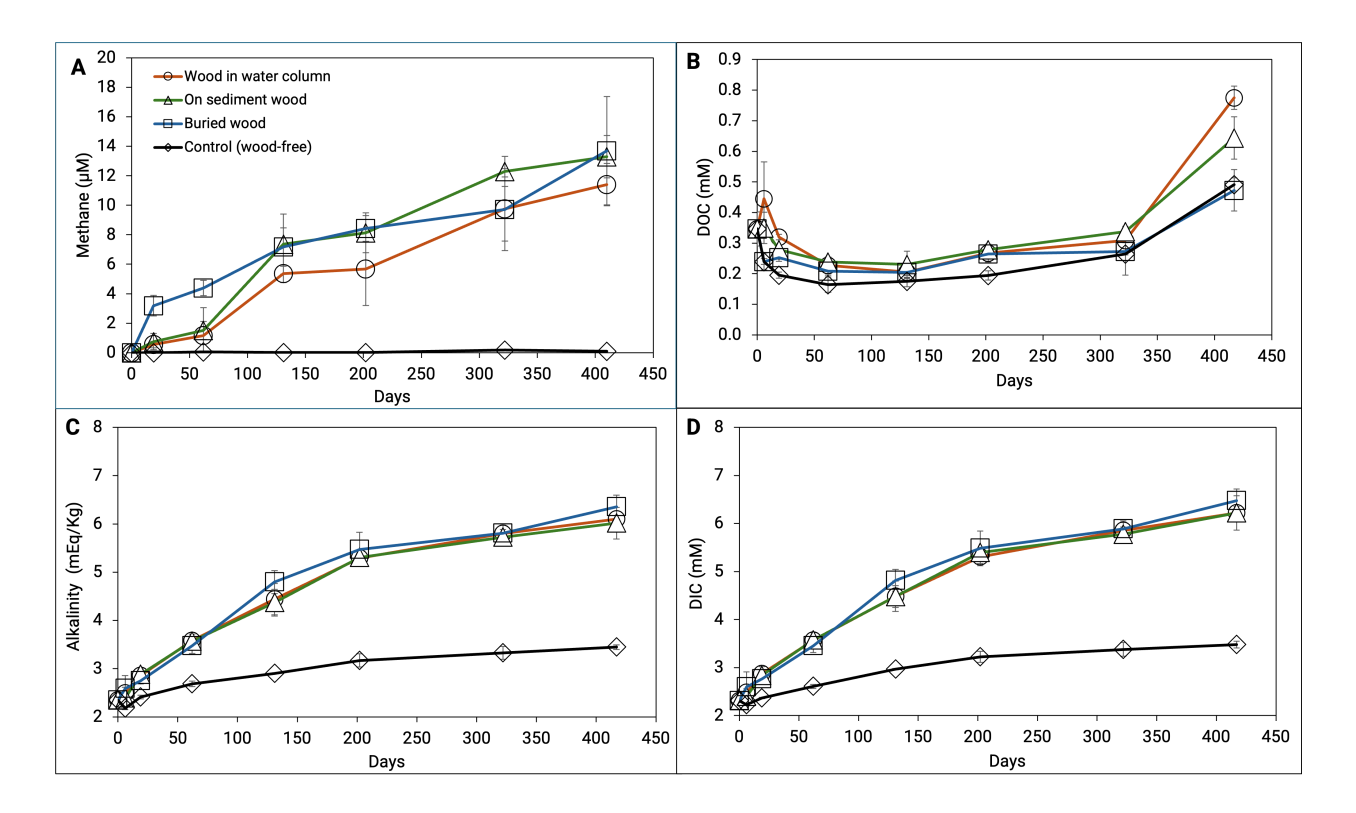


**Figure 2.** Changes in methane (A), DOC (B), alkalinity (C), and DIC (D) concentrations over time after the addition of wood to the bottles; wood in the water column, placed on the sediment-water interface, and buried in the sediment.

#### 3.2 Wood burial limits DOC fluxes

Our results indicate temporal changes in DOC concentrations of DOC, with an initial decline (0–60 days), followed by a plateau (60–131 days), and a late-stage increase (after 131 days). This increase was specific to treatments from day 200 onward. Distinct patterns emerged early: by day 6, the water-column wood had produced the highest DOC concentration (0.45  $\pm$  0.12 mM), indicating that hydrolysis and fermentation, which convert POC to DOC, outpaced DOC decomposition. In treatments with wood on the sediment, DOC levels (0.35  $\pm$  0.05 mM) were similar to the control (p = 1.0). In contrast, buried wood released DOC more slowly (0.24  $\pm$  0.01 mM), showing a slight reduction relative to the control (p = 0.06). Between days 19 and 62, all DOC values in wood additions converged to approximately 0.21–0.25 mM, whereas in the control samples, we measured 0.16  $\pm$  0.03 mM DOC, suggesting that DOC decomposition temporarily balanced production. DOC concentrations then leveled off between days 62 and 131.



At day 202, the three wood configurations stabilized at 0.27–0.28 mM, remaining statistically indistinguishable from one another (p > 0.05), yet already exceeding the control (0.19  $\pm$  0.02 mM; p < 0.05). By day 322, DOC values were: water > surface > buried  $\approx$  control, and this trend persisted till day 417. A one-way ANOVA on the day 417 values confirmed that DOC differed significantly among configurations (F<sub>(3</sub>, 8) = 21.5, p  $\approx$  0.0003); Tukey HSD post-hoc tests showed that the water-column and surface-sediment configurations were both higher than the buried-wood and no-wood controls, with the water-column treatment yielding the most significant DOC accumulation (0.78  $\pm$  0.04 mM).

We propose that the limited DOC accumulation during the first ~200 days was due to microbial DOC consumption as there was a concurrent increase in DIC, reflecting intense terminal mineralization of DOC (Figure 2D). After day 200, DIC production declined, signaling a drop in DOC consumption and DOC concentrations began to climb thereafter, implying that production exceeded removal.

As DIC production was essentially identical in all three wood-bearing configurations throughout the experiment (Figure 2D), the differences in overall mineralization rates are unlikely to explain the differences in the late-stage DOC accumulation. Instead, an additional sink that varies with the degree of wood–sediment contact must regulate how much DOC remains in solution. The most plausible sink is abiotic or microbially mediated sorption or precipitation within the sediment matrix. As DOC diffuses into pore water, it can adsorb to clay surfaces (Keil & Hedges, 1993; Mayer, 1994), co-precipitate with freshly formed iron-sulfide and iron-carbonate minerals (Lalonde et al., 2012; Wagai & Mayer, 2007; Eglinton et al., 2021), or be incorporated into refractory organic–sulfur complexes (Raven et al., 2021; Heitmann & Blodau, 2006). DOC leached from the suspended wood can bypass these sinks, escape into the overlying water and accumulate. DOC scavenging is limited when wood is placed on top of the sediments, yielding intermediate concentrations. In sediments, scavengers may use most of the DOC released from the buried wood.

#### 3.3. Wood additions result in DIC and alkalinity increase

Following previous studies in anoxic aquatic environments, DIC concentration and alkalinity increased markedly following wood additions, consistent with enhanced microbial degradation of



organic carbon under reducing conditions (Canfield et al., 1993; Burdige, 2006; Komada et al., 2016), while only a minor increase was detected in the control (Figure 2C, D). The rate of change varied with time. During the first 202 days, DIC and alkalinity in the wood treatments increased at a rate of 0.0146 mM day<sup>-1</sup> (or mEq kg<sup>-1</sup> day<sup>-1</sup>), whereas in the control, they increased at a rate of 0.0049 mM day<sup>-1</sup>. From day 202 to 410, the rates dropped to 0.0043 mM day<sup>-1</sup> and 0.0012 mM day<sup>-1</sup> in wood additions and controls, respectively (Figure 3).

In our experiment, the majority of alkalinity vs. DIC data points clustered near the 1:1 line (Figure S1), indicating a predominant influence of microbial sulfate reduction in biomass breakdown. Typically, microbial sulfate reduction generates one equivalent of alkalinity per mole of DIC, whereas microbial iron reduction exhibits a stoichiometry closer to one-to-eight (e.g., Soetaert et al., 2007). We assume that the carbonate system controlled the total alkalinity, while the contributions of ammonium and Fe<sup>2+</sup> were negligible. Consequently, the transformation of organic carbon into bicarbonate (HCO<sub>3</sub><sup>-</sup>) represents a stable form of carbon storage within the aqueous phase. Under the prevailing anoxic and near-neutral pH conditions, the produced DIC is predominantly present as bicarbonate rather than gaseous CO<sub>2</sub>, which minimizes degassing and enhances carbon retention (Berner, 1980; Millero, 2007). Because bicarbonate is readily incorporated into the dissolved carbonate system or precipitates as carbonate minerals, it remains trapped within sediments and pore waters, thereby contributing to long-term carbon sequestration (Burdige, 2006; Komada et al., 2016).



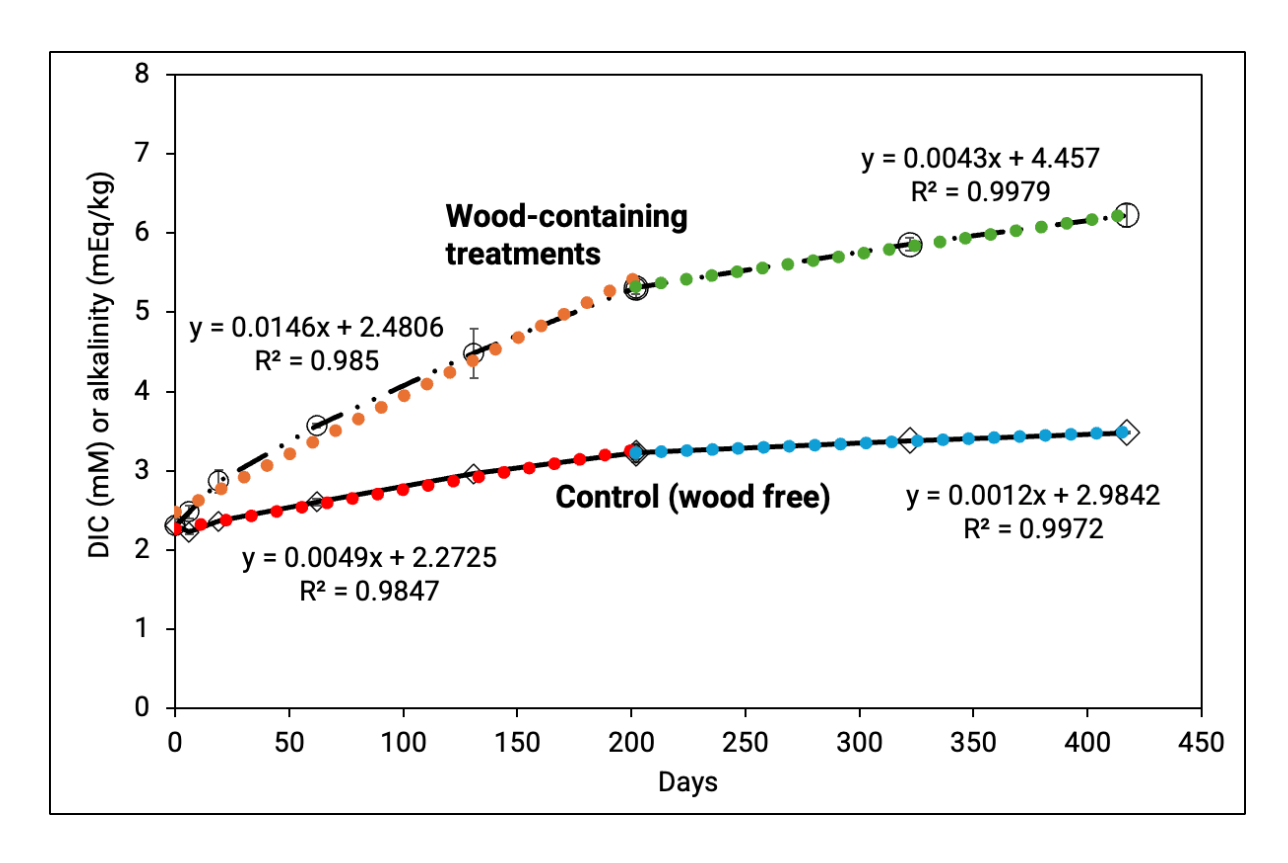


**Figure 3.** Production rates of DIC and alkalinity over time. Linear trendlines were fitted for days 0–202 and days 202–410.

#### 3.4 Mass loss from wood

A visual comparison of freezer-preserved wood pieces from T<sub>0</sub> and those retrieved after 410 days revealed no observable breakdown (Supplementary Figure S2). Mass loss measurements consistently showed high wood preservation throughout the 410-day experiment, with values ranging from approximately 96% to 99% (Figure S3). These results indicate that the wood remained largely intact throughout the study. We observed no clear decreasing trend in preservation across the different time points, suggesting that any degradation processes occurred slowly, if at all, under the experimental conditions. The stable preservation levels throughout the experiment indicate minimal decomposition. However, uncertainties in mass loss can arise from salt uptake, potential sulfurization reactions, and/or rehydration effects.

The 0.8 cm<sup>3</sup> beech-wood used in the experiment, with an initial wet mass of 400 mg and 10 % bound water (360 mg dry mass), lost 6.12 mg, that is, 1.7 % of its carbon during decomposition, yielding a final dry-wood mass of 353.88 mg (bulk density 0.442 g cm<sup>-3</sup>). Assuming a solid cell-



wall density of 1.5 g cm<sup>-3</sup>, the pore fraction is 0.7, corresponding to 0.56 cm<sup>3</sup> (563.5 mg) of seawater at saturation. After subtracting 10% bound water (35.4 mg), the net uptake was 528.2 mg, which at Black Sea salinity (20 ppt) equals 10.6 mg of retained salt. After one year of submersion and drying, the wood retained ~10.6 mg of salt, representing a 3% increase over its initial dry mass of 353.9 mg. This mass change lies within the 1–4% range of decomposition estimates based on dry-mass loss, highlighting the ambiguity of using dry mass alone to assess decomposition.

After 410 days of anoxic incubation, the wood carbon content declined from its initial value ( $T_0 = 46.57 \pm 0.26 \%$  C) in all three configurations (Figure S4). Carbon content decreased as follows: i) wood in the water column dropped to  $44.41 \pm 0.44 \%$  C, corresponding to a loss of  $4.64 \pm 1.10 \%$ ; ii) wood on the sediment surface to  $44.17 \pm 1.16 \%$  C, a loss of  $5.15 \pm 2.55 \%$ ; and iii) buried wood to  $44.13 \pm 0.08 \%$  C, a loss of  $5.24 \pm 0.58 \%$  C. The near-identical mean values across configurations indicates that anoxic decomposition produced similar carbon losses from the wood. On average, the three configurations resulted in a carbon loss of approximately 5% over the 410-day incubation period. When considering losses based on changes in DOC, DIC, and methane, all three configurations yielded an overall loss of  $1.68 \pm 0.22 \%$  carbon after 410 days under anoxia. The remaining  $\sim 3\%$  difference may reflect such sinks such as incorporation of degradation products into microbial biomass, sorption of dissolved organic compounds to mineral surfaces, formation of refractory organic—sulfur complexes, or partial conversion into solid-phase carbonate or iron-bound carbon pools within the sediment matrix.

### 3.5 Wood addition boosted sulfate depletion

Over the first two months (Day 0–62), all three types of wood addition stimulated sulfate consumption (sulfate reduction) more than the wood-free control (Figure S5). Between Day 62 and Day 322, we observed a marked sulfate depletion following wood addition (a decrease to circa 71.5%, as opposed to 76.5% in controls). In the final interval (Day 322–410), the control plateaued at 76.3%, whereas the wood additions continued to consume sulfate more gradually, reaching  $\sim$ 70%. By Day 410, sulfate concentrations in all wood-containing treatments were significantly lower than in the control ( $t_{(2)} = 13.4–23.2$ , p < 0.01), corresponding to a removal of approximately 29–31% of the initial sulfate compared to only  $\sim$ 24% in the wood-free bottles. Sulfate depletion



in both wood additions and controls suggests that degradation of organic matter present in both the water column and sediment is likely the primary driver of sulfate reduction. Wood degradation supplemented organics to sulfate-reducing bacteria, accelerating sulfate reduction compared to the wood-free control (19.8 vs 18.2–18.4mM in controls and wood additions, respectively, out of the initial 26 mM sulfate, circa 5% difference). In turn, sulfide measurements were below the  $0.02~\mu\text{M}$  detection limit of the applied analytical method (data not shown). The absence of detectable dissolved sulfide is likely attributable to its rapid reaction with iron minerals present in the sediment, leading to the formation of iron sulfide minerals. A layer of dark particles that formed on the sediment surface during the experiment supported these indications (Figure S6).

# 3.6 Wood additions affected the composition and function of the microbial community

Despite pronounced shifts in bacterial community structure, alpha diversity remained remarkably stable across treatments and timepoints (Figure S7). The Shannon index averaged 6.2 with a standard deviation of  $\pm 0.2$ , and the Simpson index consistently remained high at approximately 0.996, indicating that all communities retained a high degree of richness and evenness throughout the 14-month incubation period. Microbial communities resembled those of natural anoxic sediments in the nearshore Mediterranean Sea (Rubin-Blum et al., 2022), with dominant anaerobic taxa, including Anaerolineales, Syntrophobacterales, and Bathyarchaea, among others (Figure S8). Most taxa were prevalent across the treatments. Key functional groups included fermenters and sulfate reducers; however, the assumed functional diversity of these communities appears to be complex. We observed a marked shift in communities compared to those at the beginning of the experiment (t0), while responses were heterogeneous among individual treatments (Figure 4A). By the end of the experiment, we identified significant changes between wood additions and controls (PERMANOVA:  $R^2 = 0.085$ , F = 2.04, P = 0.001, Figure 4B).

Analysis of differentially abundant genera revealed functional signals that mirrored the biogeochemical processes occurring in the incubation (Figures 5 and S9, Supplementary Tables S1 and S2). Genera that can perform both hydrolysis and fermentation were enriched in the wood treatments compared to the controls. *Defluviitalea*, a known cellulolytic fermenter, emerged as the strongest indicator species across all wood configurations, suggesting that the breakdown of lignocellulosic material provided a steady supply of substrates for fermentation. Unclassified



Fibrobacterales were abundant only in wood-treated bottles, reinforcing the role of specialized fermenters in initiating the decomposition process.

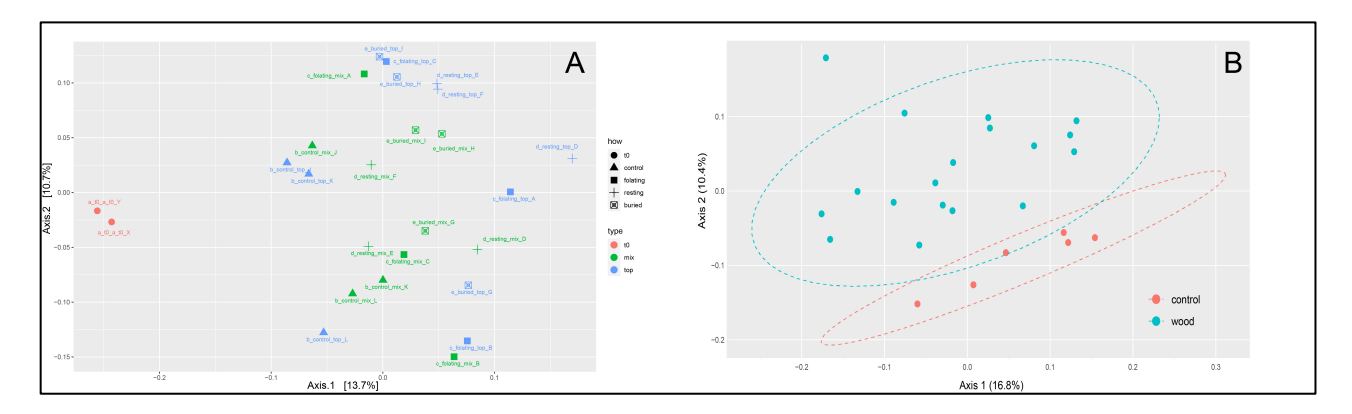


**Figure 4.** Principal coordinates analyses (PCoA) based on the read abundance of OTUs (day 410) per sample (A) and with t0 excluded (B).

Consistent with the availability of fermentation byproducts, sulfate-reducing taxa, including Sva1033 within Desulfuromonadales, were more abundant in the presence of wood. This observation aligns with the stoichiometric evidence from DIC and alkalinity production, which indicates that sulfate reduction is the dominant terminal electron-accepting pathway. The indicator species analysis corroborated these patterns, showing associations between fermentative and sulfate-reducing lineages and the wood-amended treatments. Methylotrophic methanogenic archaea, particularly *Methanococcoides*, were identified as indicator species for wood treatments. However, their relative abundance was lower than that of sulfate reducers, reflecting the known thermodynamic preference for sulfate reduction in marine sediments rich in sulfate. We note that the diversity of methylotrophic metanogens can be broader, as exemplified by some members of the very abundant Candidatus Bathyarchaeota (Thermoproteota), which can perform methylotrophic methanogenesis (Evans et al., 2015; Schorn et al., 2022). Taken together, these results demonstrate a robust microbial succession that begins with hydrolysis and fermentation of wood material, followed by consumption of fermentation products via sulfate reduction and, to a lesser extent, methanogenesis.



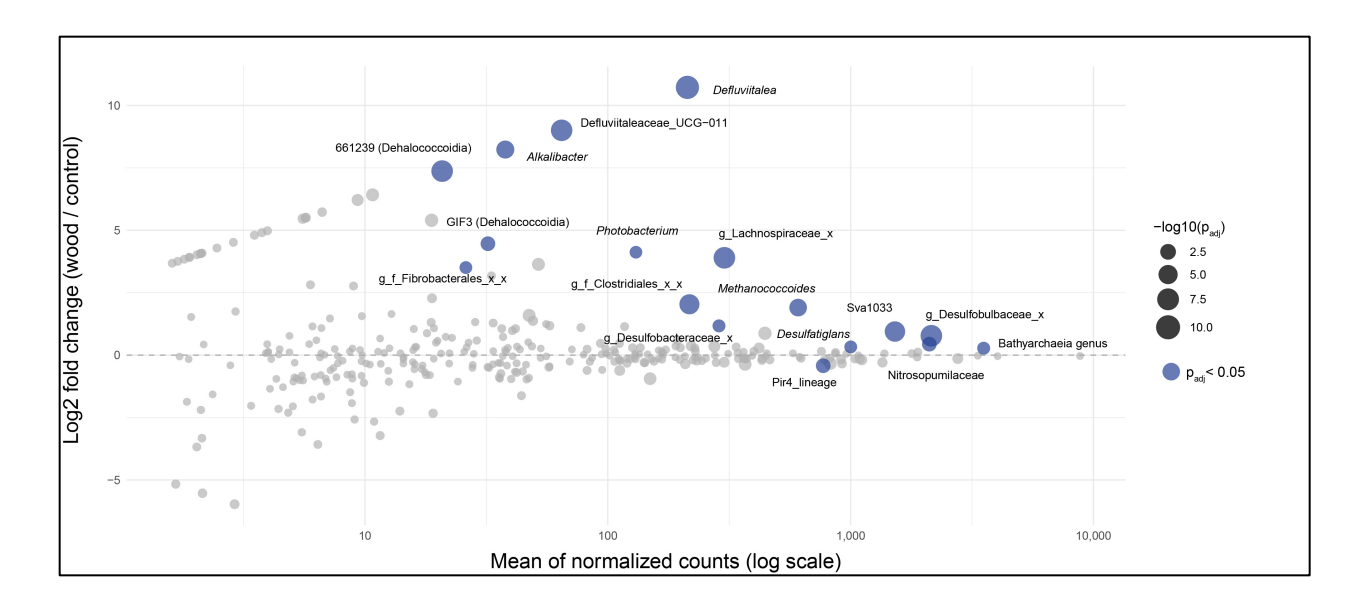


**Figure 5.** MA plot showing log2 fold changes and significance of genera, comparing all the wood addition treatments with controls (T0 excluded). The x-axis shows read abundance, and the y-axis is the log2-fold change (larger positive numbers suggest a more substantial enrichment in wood additions). Circle size correlates with the inverse log of the adjusted p-value (larger circles imply more significant change).

Using taxonomy-based inference, we identified enrichment of specific KEGG Orthology (KO) molecular functions in wood-treated samples (Figure S10A, Supplementary Table S3). These included genes encoding functions associated with quorum sensing (e.g., *cqsA*), fatty acid metabolism (e.g., *luxC*), sugar transporters (e.g., *alsA* and *alsC*), and osmoprotectant synthesis (e.g., *otsA*). Carbohydrate metabolism was one of the most enriched at the second-tier functional categories (n = 270), suggesting a robust response of sugar-degrading microbial functions to wood addition. We found that the putative chitin disaccharide deacetylase (*deaA*) is one of the functions markedly enriched in wood additions, as detected by DESeq2, highlighting the role of polysaccharide degradation as a key process following wood additions. This supports the hypothesis that wood-amended communities were restructured to enable enhanced transport and metabolism of lignocellulosic substrates.

The top 20 differentially abundant MetaCyc pathways also pointed to carbohydrate-related and energy-yielding processes (Figure S10B, Supplementary Table S4). Pathways like glycolysis V (P341), hexitol degradation (HEXTOLDEGSUPER-PWY), and the TCA cycle (7254) were enriched in wood, along with superpathways of menaquinone biosynthesis (5897-5899). These changes indicate a shift toward increased sugar fermentation and enhanced metabolic capacity in the wood-associated microbiomes. Enrichment of cholesterol and xylose degradation pathways



further supports a trend toward microbial specialization in the breakdown of complex organic matter.

Several KO features and one MetaCyc pathway support the presence of methylotrophic methanogenesis, likely associated with methanogenic archaea, such as Methanococcoides. Among the significantly enriched KOs were those annotated as methylated compound-specific enzymes, including methyltransferases (e.g., mtsB), S-adenosylmethionine (AdoMet)-dependent methyltransferases, and enzymes directly related to methanogenesis, such as formylmethanofuran dehydrogenase (fwdC). Additionally, the methanogenesis MetaCyc pathway showed significant enrichment in wood-amended samples ( $p_{adj} = 0.008$ ), indicating increased capacity for methane production via methylotrophic routes.

#### 4. Conclusions

Across 14 months of anoxic incubation, wood burial showed impressive preservation: >97.5% carbon retained, based on C content, ~98.3% via carbon budgets, and >96% by dry mass. The strong 1:1 relationship between DIC and alkalinity, the minimal methane relative to DIC, and the rapid sulfide immobilization indicate that sulfate reduction is the dominant terminal pathway. Microbial analyses confirmed a shift toward fermenters and sulfate reducers, with methanogens playing a limited role, consistent with the geochemical evidence.

Despite these promising findings, this study has significant limitations. The closed-bottle design cannot fully reproduce natural gradients, transport processes, or sediment heterogeneity. Salt uptake and sulfurization complicate dry-mass loss estimates. We tested only a single biomass type and block size, and the 410-day duration is short compared to the decadal to centennial scales relevant for carbon storage.

Importantly, our original hypothesis that decomposition rates of organic matter depend on its position - whether buried in sediment, lying on the sediment surface, or suspended in the water column - was not supported by the results. Under anoxic conditions, wood showed similarly low decomposition regardless of placement, suggesting that intrinsic chemical recalcitrance and microbial community composition, rather than position alone, govern preservation.



Future work should extend incubations, explore diverse biomass types and sizes, and test natural field conditions in anoxic basins. Linking microbial succession to carbon fluxes in real-world settings will be crucial for validating durability and environmental stability. Scaling experiments and field trials will ultimately determine whether anoxic marine burial of lignocellulosic biomass can serve as a robust, low-risk strategy for long-term carbon dioxide removal.

#### **Author contribution**

NA, HL, PK and DA conceived the study and acquired funding. NA, HL, PK and DA performed the experiments and analyzed the data. MR-B analyzed NGS data. NA, MR-B and DA wrote the paper with contributions from other authors

# Acknowledgments

We are grateful to Dr. Gilad Antler (Ben-Gurion University of the Negev / IUI, Israel), Prof. Morgan Reed Raven (University of California, Santa Barbara), Prof. Tina Treude (UCLA), Prof. Alexey Kamyshny (Ben-Gurion University of the Negev, Israel), Dr. Gustavo A. Ramírez (California State University, Los Angeles), and Dr. Dan Vasiliu (GeoEcoMar, Romania) for their thoughtful reviews and valuable feedback. Their insightful comments and suggestions substantially improved the manuscript.

#### References

Andersen, K. S., Kirkegaard, R. H., Karst, S. M., & Albertsen, M. (2018). *ampvis2: An R package to analyse and visualise 16S rRNA amplicon data. bioRxiv*, 299537. https://doi.org/10.1101/299537

Apprill, A., McNally, S., Parsons, R., & Weber, L. (2015). Minor revision to V4 region SSU rRNA 806R gene primer greatly increases detection of SAR11 bacterioplankton. *Aquatic Microbial Ecology*, 75(2), 129–137. https://doi.org/10.3354/ame01753

Archer, D., Emerson, S., & Reimers, C. (1998). Dissolution of calcite in deep-sea sediments: pH and O<sub>2</sub> microelectrode results. *Geochimica et Cosmochimica Acta*, 52, 2835–2845.

Berner, R. A. (1980). Early diagenesis: A theoretical approach. Princeton University Press.

Berner, R. A. (1981). A new geochemical classification of sedimentary environments. *Journal of Sedimentary Petrology*, 51, 359–365.

Beulig, F., Røy, H., Glombitza, C., & Jørgensen, B. B. (2018). Control on rate and pathway of anaerobic organic carbon degradation in the seabed. *Proceedings of the National Academy of Sciences*, 115, 367–372. https://doi.org/10.1073/pnas.1715789115



Burdige, D. J. (2006). Geochemistry of marine sediments. Princeton University Press.

Canfield, D. E. (1994). Factors influencing organic carbon preservation in marine sediments. *Chemical Geology*, 114, 315–329. https://doi.org/10.1016/0009-2541(94)90061-2

Canfield, D. E., Thamdrup, B., & Hansen, J. W. (1993). The anaerobic degradation of organic matter in Danish coastal sediments: Iron reduction, manganese reduction, and sulfate reduction. *Geochimica et Cosmochimica Acta*, 57, 3867–3883.

Canfield, D. E., Thamdrup, B., & Kristensen, E. (2005). Heterotrophic carbon metabolism. *Advances in Marine Biology*, 48, 293–379. https://doi.org/10.1016/S0065-2881(05)48005-0

Cline, J. D. (1969). Spectrophotometric determination of hydrogen sulfide in natural waters. *Limnology and Oceanography*, 14(3), 454–458. https://doi.org/10.4319/lo.1969.14.3.0454

Crill, P. M., & Martens, C. S. (1986). Methane production from acetate and associated methane fluxes from anoxic coastal sediments. *Limnology and Oceanography*, 31(4), 831–844. https://doi.org/10.4319/lo.1986.31.4.0831

De Cáceres, M., & Legendre, P. (2009). Associations between species and groups of sites: Indices and statistical inference. *Ecology*, 90, 3566–3574. https://doi.org/10.1890/08-1823.1

Douglas, G. M., Maffei, V. J., Zaneveld, J. R., Yurgel, S. N., Brown, J. R., Taylor, C. M., et al. (2020). PICRUSt2 for prediction of metagenome functions. *Nature Biotechnology*, 38, 685–688. https://doi.org/10.1038/s41587-020-0548-6

Eglinton, T. I., Hemingway, J. D., & Dickens, A. F. (2021). Organic carbon–mineral interactions in marine sediments. *Annual Review of Earth and Planetary Sciences*, 49, 249–278. https://doi.org/10.1146/annurevearth-081420-063843

Evans, P. N., Parks, D. H., Chadwick, G. L., Robbins, S. J., Orphan, V. J., Golding, S. D., & Tyson, G. W. (2015). Methane metabolism in the archaeal phylum *Bathyarchaeota* revealed by genome-centric metagenomics. *Science*, 350, 434–438. https://doi.org/10.1126/science.aac7745

Fenchel, T., & Finlay, B. J. (1995). Ecology and evolution in anoxic worlds. Oxford University Press.

Froelich, P. N., Klinkhammer, G. P., Bender, M. L., Luedtke, N. A., Heath, G. R., Cullen, D., et al. (1979). Early oxidation of organic matter in pelagic sediments of the eastern equatorial Atlantic: Suboxic diagenesis. *Geochimica et Cosmochimica Acta*, 43(7), 1075–1090.

Glöckner, F. O., Yilmaz, P., Quast, C., et al. (2017). 25 years of serving the community with ribosomal RNA gene reference databases and tools. *Nucleic Acids Research*, 45(D1), D1–D7. https://doi.org/10.1093/nar/gkw971

Gobas, F. A., & MacLean, L. G. (2003). Sediment–water distribution of organic contaminants in aquatic ecosystems: The role of organic carbon mineralization. *Environmental Science & Technology*, 37(4), 735–741. https://doi.org/10.1021/es0258031



Hee, C. A., Pease, T. K., Alperin, M. J., & Martens, C. S. (2001). Dissolved organic carbon production and consumption in anoxic marine sediments: A pulsed-tracer experiment. *Limnology and Oceanography*, 46(8), 1908–1920. https://doi.org/10.4319/lo.2001.46.8.1908

Heitmann, T., & Blodau, C. (2006). Oxidation and incorporation of hydrogen sulfide by dissolved organic matter. *Chemical Geology*, 235, 12–20. https://doi.org/10.1016/j.chemgeo.2006.06.015

IPCC. (2023). Climate change 2023: Synthesis report. IPCC.

Jørgensen, B. B. (2000). Bacteria and marine biogeochemistry. In H. D. Schulz & M. Zabel (Eds.), *Marine Geochemistry* (pp. 173–207). Springer.

Keil, R. G., & Hedges, J. I. (1993). Sorptive preservation of labile organic matter in marine sediments. *Nature*, 361, 686–688. https://doi.org/10.1038/361686a0

Keil, R. G., Nuwer, J. M., & Strand, S. E. (2010). Burial of agricultural byproducts in the deep sea as a form of carbon sequestration: A preliminary experiment. *Marine Chemistry*, 122(1–4), 91–95. https://doi.org/10.1016/j.marchem.2010.07.002

Komada, T., Burdige, D. J., & Li, H. (2016). Organic matter diagenesis and sediment—water exchange in the Santa Monica Basin, California: Carbon and nitrogen cycling. *Deep-Sea Research Part I*, 115, 20–34. https://doi.org/10.1016/j.dsr.2016.05.010

Lalonde, K., Mucci, A., Ouellet, A., & Gélinas, Y. (2012). Preservation of organic matter in sediments promoted by iron. *Nature*, 483, 198–200. https://doi.org/10.1038/nature10855

Love, M. I., Huber, W., & Anders, S. (2014). Moderated estimation of fold change and dispersion for RNA-seq data with DESeq2. *Genome Biology*, 15, 550. https://doi.org/10.1186/s13059-014-0550-8

Lovley, D. R., & Phillips, E. J. P. (1987). Competitive mechanisms for inhibition of sulfate reduction and methane production in the zone of ferric iron reduction in sediments. *Applied and Environmental Microbiology*, 53(11), 2636–2641.

Maltby, J., Sommer, S., Dale, A. W., et al. (2018). Microbial methane production fuels massive sulfide formation in organic-rich marine sediments. *Nature Communications*, 9, 5179. https://doi.org/10.1038/s41467-018-07655-9

Mayer, L. M. (1994). Surface area control of organic carbon accumulation in continental shelf sediments. *Geochimica et Cosmochimica Acta*, 58, 1271–1284. https://doi.org/10.1016/0016-7037(94)90381-6

Megonigal, J. P., Hines, M. E., & Visscher, P. T. (2003). Anaerobic metabolism: Linkages to trace gases and aerobic processes. In W. H. Schlesinger (Ed.), *Biogeochemistry* (pp. 317–424). Elsevier.

Middelburg, J. J., & Levin, L. A. (2009). Coastal hypoxia and sediment biogeochemistry. *Biogeosciences*, 6(7), 1273–1293. https://doi.org/10.5194/bg-6-1273-2009

Millero, F. J. (2007). The marine inorganic carbon cycle. *Chemical Reviews*, 107, 308–341. https://doi.org/10.1021/cr0503557



National Academies of Sciences, Engineering, and Medicine. (2021). A research strategy for ocean-based carbon dioxide removal and sequestration. National Academies Press.

Oremland, R. S., Marsh, L. M., & Polcin, S. (1982). Methane production and simultaneous sulphate reduction in anoxic, salt marsh sediments. *Nature*, 296, 143–145. https://doi.org/10.1038/296143a0

Parada, A. E., Needham, D. M., & Fuhrman, J. A. (2016). Every base matters: Assessing small-subunit rRNA primers for marine microbiomes with mock communities, time series and global field samples. *Environmental Microbiology*, 18(5), 1403–1414. https://doi.org/10.1111/1462-2920.13023

R Core Team. (2024). R: A language and environment for statistical computing. R Foundation for Statistical Computing.

Raven, M. R., Keil, R. G., Webb, S. M., & Fike, D. A. (2021). Organo-sulfur formation in sediments through reactive iron phases and reduced sulfur species. *Nature Geoscience*, 14, 791–797. https://doi.org/10.1038/s41561-021-00816-8

Raven, M. R., Crotteau, M., Evans, N., Girard, Z. C., Martinez, A., Young, I. S., & Valentine, D. L. (2023). Biomass storage in anoxic marine basins: Initial estimates of geochemical impacts and CO<sub>2</sub> sequestration capacity. *Authorea Preprints*. https://doi.org/10.22541/au.169947201.11394073/v1

Reeburgh, W. S. (2007). Oceanic methane biogeochemistry. *Chemical Reviews*, 107, 486–513. https://doi.org/10.1021/cr050362v

Rubin-Blum, M., Sisma-Ventura, G., Yudkovski, Y., Belkin, N., Kanari, M., Herut, B., et al. (2022). Diversity, activity, and abundance of benthic microbes in the Southeastern Mediterranean Sea. *FEMS Microbiology Ecology*, 98, fiac009. https://doi.org/10.1093/femsec/fiac009

Sela-Adler, M., Ronen, Z., Herut, B., Antler, G., Vigderovich, H., Eckert, W., & Sivan, O. (2015). Co-existence of methanogenesis and sulfate reduction with common substrates in sulfate-rich estuarine sediments. *Frontiers in Microbiology*, 6, 1421. https://doi.org/10.3389/fmicb.2015.01421

Schorn, S., Zarzycki, J., Vogt, J., et al. (2022). Methylotrophic methanogenesis in *Bathyarchaeia*. *Nature Microbiology*, 7, 1059–1068. https://doi.org/10.1038/s41564-022-01153-3

Soetaert, K., Hofmann, A. F., Middelburg, J. J., Meysman, F. J., & Greenwood, J. (2007). Reprint of "The effect of biogeochemical processes on pH." *Marine Chemistry*, 106(1–2), 380–401. https://doi.org/10.1016/j.marchem.2007.06.008

Treude, T. (2011). Biogeochemical reactions in marine sediments underlying anoxic water bodies. In *Anoxia: Evidence for Eukaryote Survival and Paleontological Strategies* (pp. 17–38). Springer.

Wagai, R., & Mayer, L. M. (2007). Sorptive stabilization of organic matter in soils by hydrous iron oxides. *Geochimica et Cosmochimica Acta*, 71, 25–35. https://doi.org/10.1016/j.gca.2006.08.047

Wright, R. J., & Langille, M. G. I. (2025). PICRUSt2-SC: An update to the reference database used for functional prediction within PICRUSt2. *Bioinformatics*, 41, btaf269. https://doi.org/10.1093/bioinformatics/btaf269



McMurdie, P. J., & Holmes, S. (2013). phyloseq: An R package for reproducible interactive analysis and graphics of microbiome census data. *PLOS ONE*, 8(4), e61217. <a href="https://doi.org/10.1371/journal.pone.0061217">https://doi.org/10.1371/journal.pone.0061217</a>



# **Supplementary Figures**

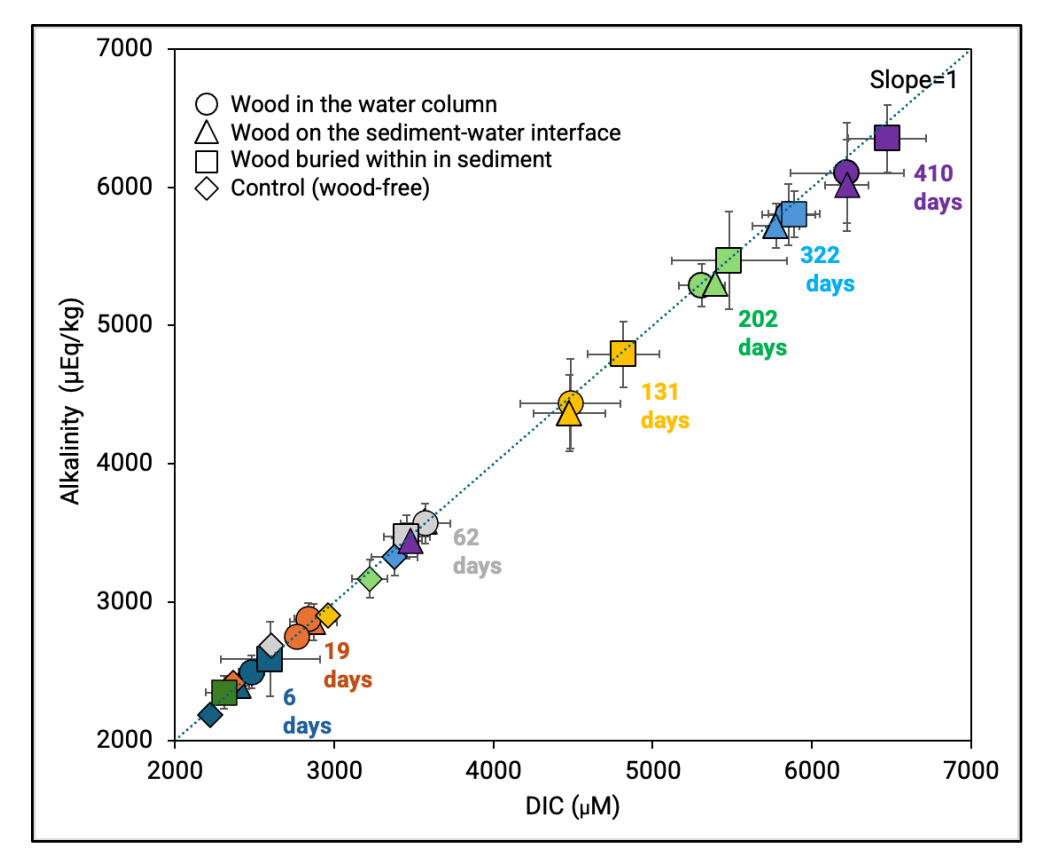


**Figure S1.** Alkalinity vs. DIC concentrations change over time. Different colors represent different sampling times, as indicated by the labels adjacent to the data points.

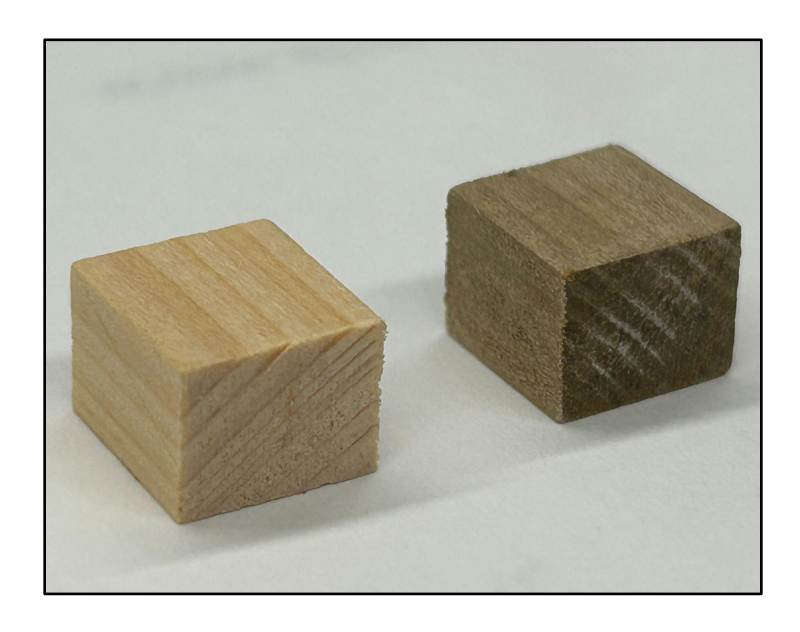




**Figure S2.** Visual comparison of wood pieces at T0 (left) and after 410 days (right), showing no observable breakdown under anoxic incubation.

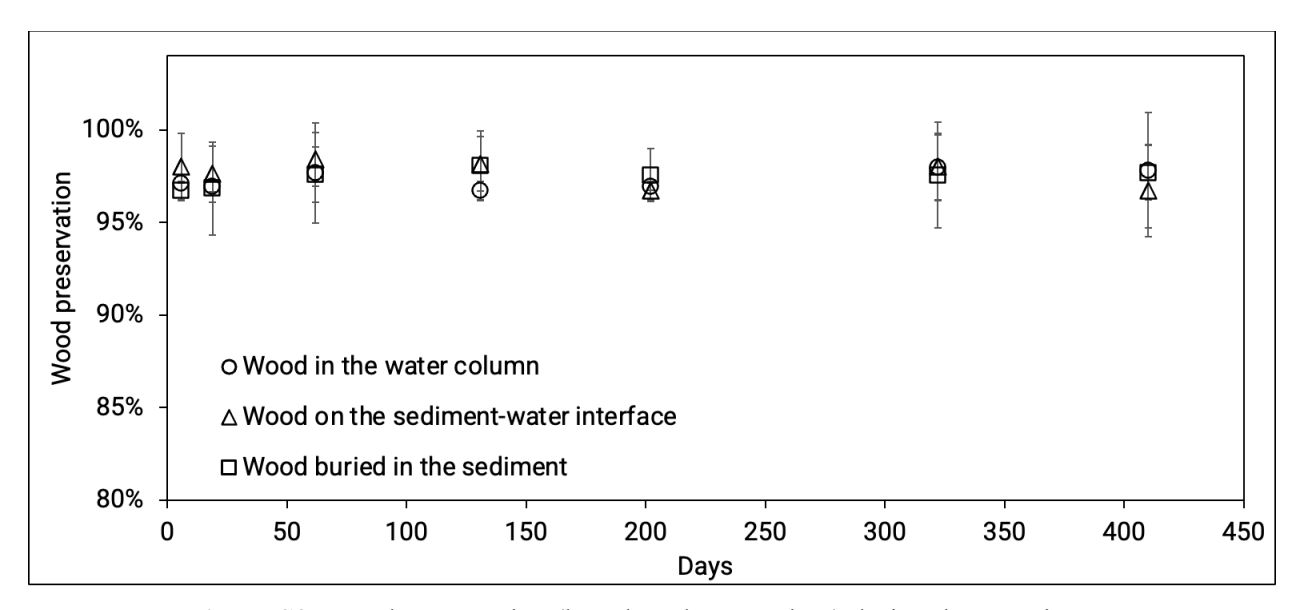
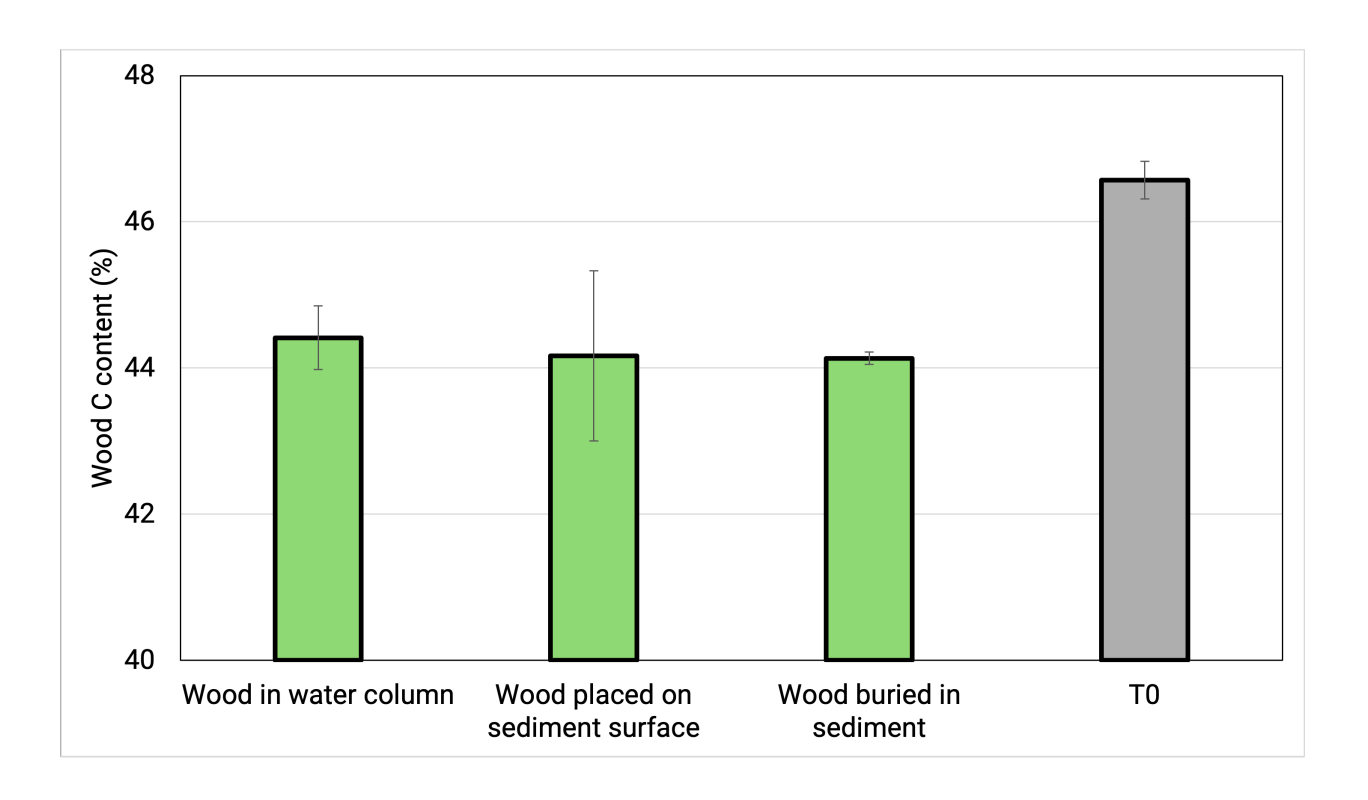
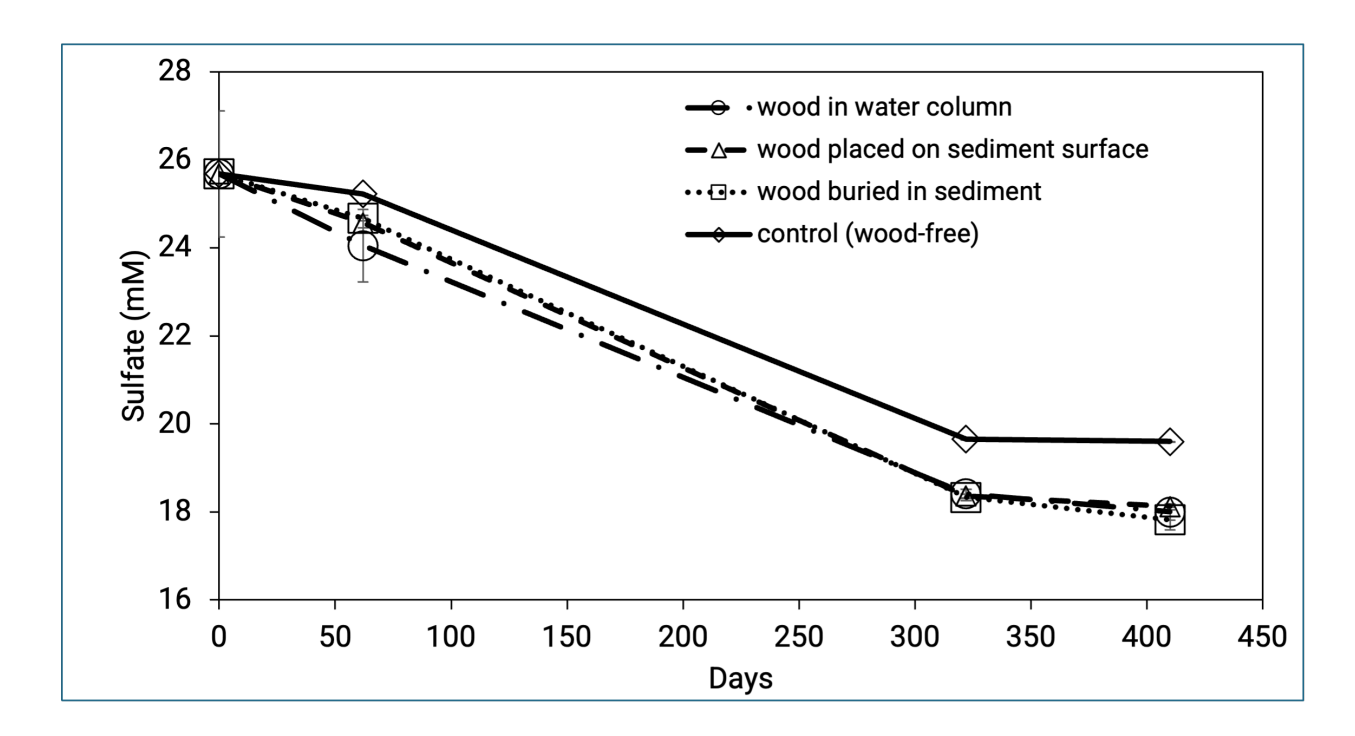


Figure S3. Wood preservation (based on dry mass loss) during the experiment.





**Figure S4.** Mean wood carbon content (± SD) after 410 days of anoxic incubation under three wood configurations (suspended, surface-placed, buried), compared to the initial (T0) wood.



**Figure S5.** Changes in sulfate concentrations over time after the addition of wood to the bottles: wood in the water column, placed on the sediment-water interface, and buried in the sediment.



**Figure S6.** A dark layer formed on the sediment surface (located in the red box); possibly iron-sulfide minerals precipitate.



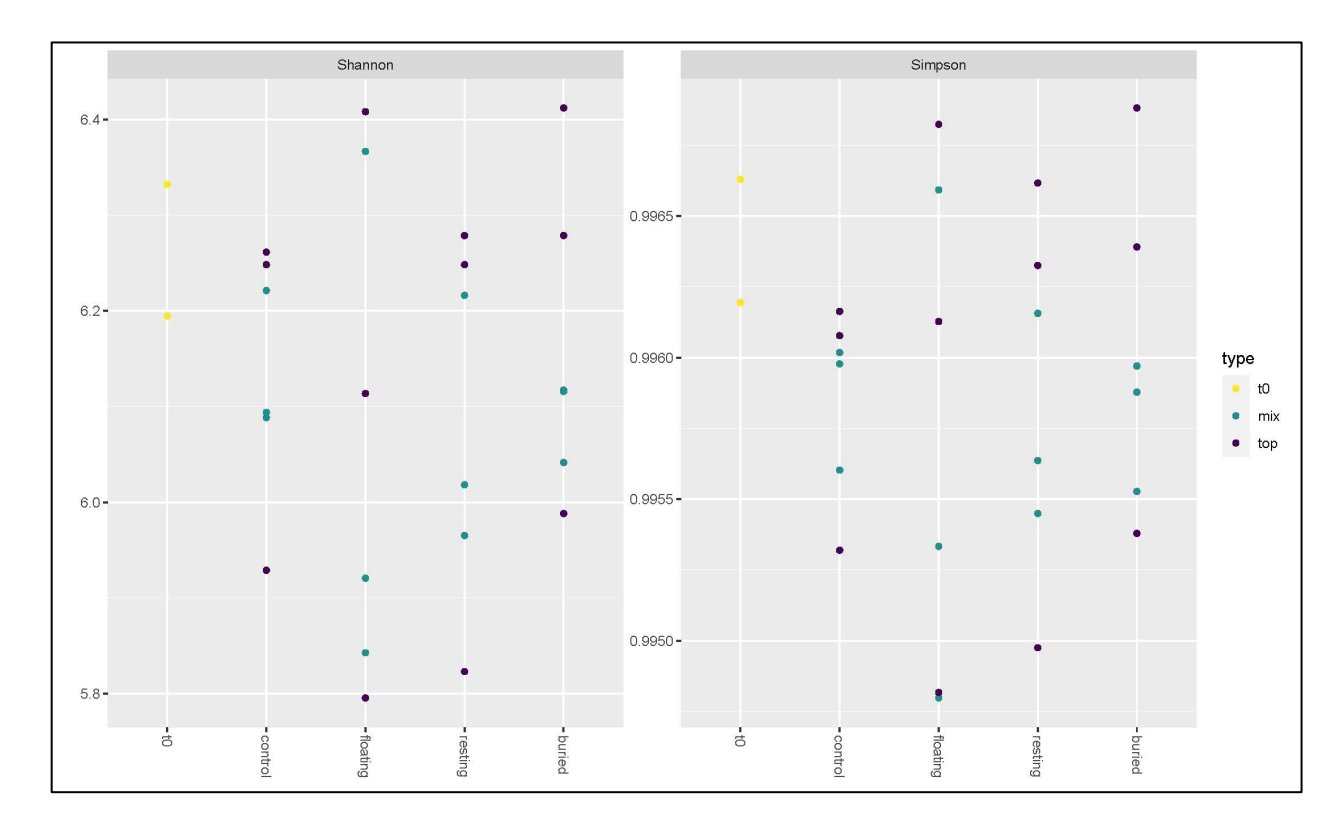


**Figure S7.** Shannon and Simpson diversity indices across treatments. Alpha diversity metrics were consistently high across all treatments and timepoints. The Shannon index averaged  $6.2 \pm 0.2$ , indicating rich and even communities. Kruskal-Wallis tests showed no significant differences in alpha diversity among treatments (p = 0.84).



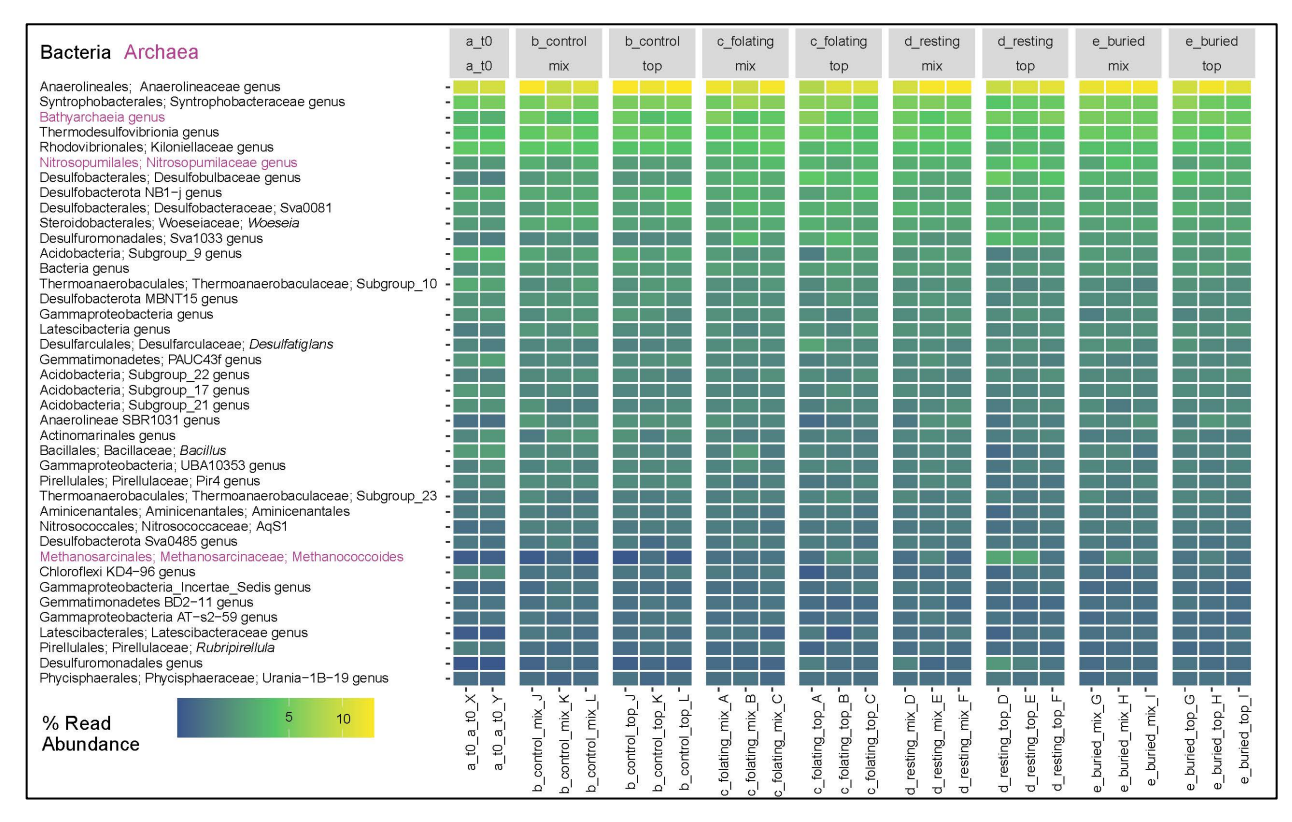


**Figure S8.** Heatmap of genus-level taxonomic composition, based on read abundance. Obligate anaerobes, including fermenters and sulfate-reducing bacteria, dominated communities. Notable taxa included Anaerolineales, Desulfobacterota, and Desulfuromonadales. Methanogenic archaea such as *Methanococcoides* were detected, suggesting potential for methane production.



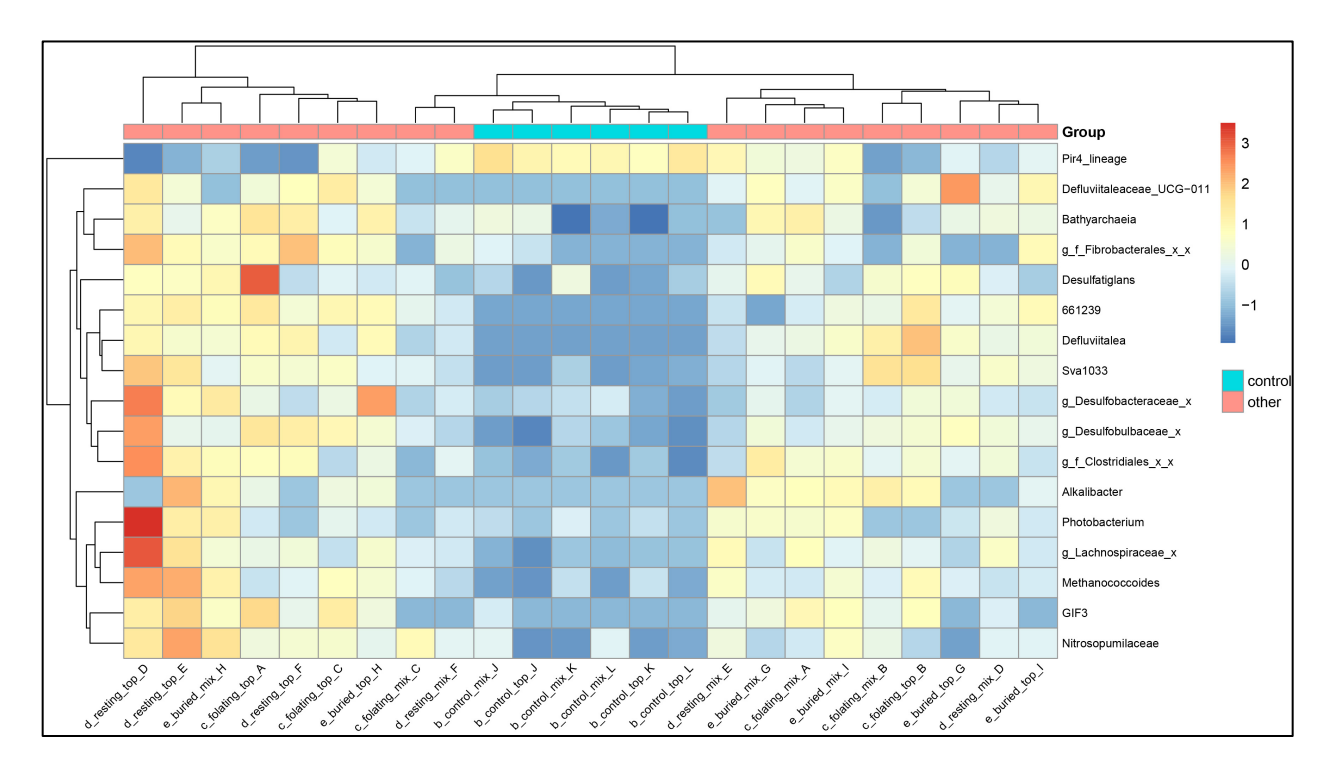
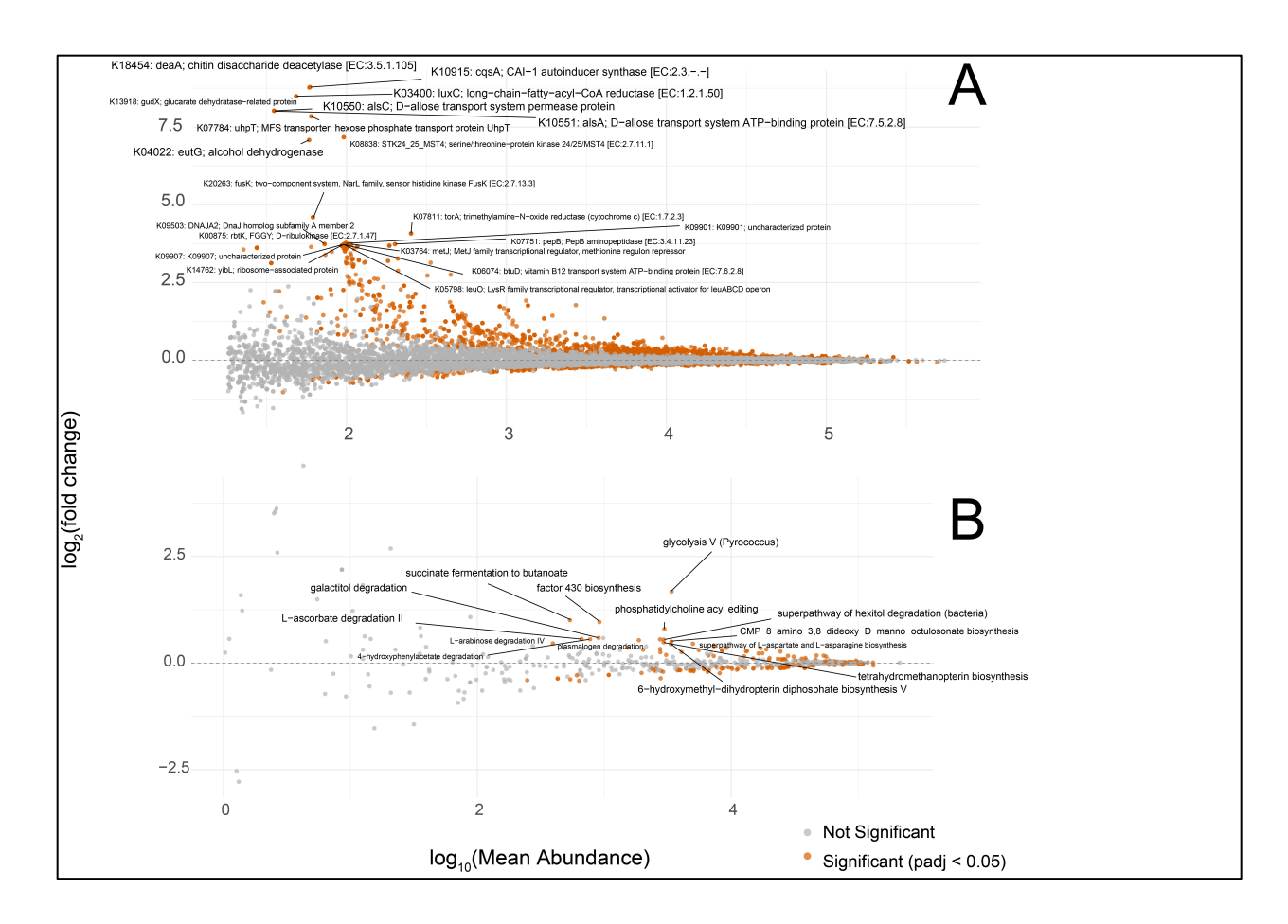


Figure S9. Heatmap of the top 20 differentially abundant genera between control and wood treatments. Genera were identified using DESeq2, comparing control samples (n = 6) to all wood treatments combined (n = 18). Read counts were  $\log_{10}$ -transformed  $[\log_{10}(\operatorname{count} + 1)]$  and then row-scaled (z-score across samples) so that each genus has a mean of zero and standard deviation of one. Color intensity reflects relative abundance compared to the mean abundance of each genus (red: above average; blue: below average). Rows (genera) and columns (samples) were clustered by hierarchical clustering using Euclidean distance and complete linkage. The annotation bar shows sample grouping (control vs wood).





**Figure S10.** MA plot of KO (A) and MetaCyc pathways (B) differential abundance based on DESeq2 analyses following Picrust2 definitions. Each point represents a KO or MetaCyc pathway, colored by adjusted p-value. The top 20 KOs / 15 MetaCyc pathways are labeled by their description.

# Supplementary tables (Excel files):

**Table S1**: Indicator species analyses, highlighting i) families enriched per experimental group; ii) genera enriched per experimental group and, iii) genera enriched when the combined wood additions were compared to controls.

Table S2: DESeq2 analyses, highlighting OTUs significantly enriched in wood additions.

Table S3: DESeq2 analyses of KEGG KO enrichment in wood additions and controls.

**Table S4**: DESeq2 analyses of MetaCyc pathways enrichment in wood additions and controls.